Journal of Electrotechnology, Electrical Engineering and Management (2025)
Clausius Scientific Press, Canada
DOI: 10.23977/jeeem.2025.080121
ISSN 2560-6697 Vol. 8 Num. 1

# *Design and Experiment of a Small-Scale Continuous Operation Planter for Pueraria Thomsonii Benth*

**Wei Luo[1,a], Qianxun Meng[1,b], Dawei Zhang[1,c], Junlin Huang[1,d], Jiajun Tang[1,e], Muhan Wu[1,f], Yu Cheng[1,g,*], Wei Lu[1,h]**

*[1]School of Mechanical and Electrical Engineering, Guilin University of Electronic Technology, Guilin, Guangxi, China*
*[a]3140514436@qq.com, [b]1309214562@qq.com, [c]2672836044 @qq.com, [d]E1791512826@qq.com, [e]820912216@qq.com, [f]1514655367@qq.com, [g]cheng19971223@qq.com, [h]lujunqi2001@163.com*
*[*]Corresponding author*

***Keywords:*** Pueraria thomsonii Benth, Small-scale planter, Microcontroller, Soil-drilling mechanism

***Abstract:*** To address the issues of nearly full manual operation in the current planting and harvesting processes of Pueraria thomsonii Benth, extremely low mechanization level, as well as the existing aging population and rising labor costs, a small-scale Pueraria thomsonii Benth planter has been designed. This planter is suitable for planting Pueraria thomsonii Benth in various field environments. Controlled by a single-chip microcontroller, it performs four key functions: soil-drilling, bag-opening, seedling placement, and irrigation during the planting process. This reduces manual labor, effectively lowers labor costs, and minimizes health hazards during planting. Considering the need for clean energy, the product adopts an electric motor as its primary power source, featuring the advantage of minimal environmental pollution.

## 1. Introduction

*Pueraria thomsonii Benth* is a typical root crop cultivated in fragmented and complex field conditions[1]. At present, its planting operation still relies mainly on manual labor, resulting in low efficiency and high labor intensity[2]. Existing planting machinery is generally designed for large-scale and standardized farmland, and is difficult to adapt to the small plots and complex terrain typical of *Pueraria thomsonii* cultivation. Consequently, the lack of compact and dedicated planting equipment has become a key engineering constraint limiting planting efficiency and mechanization level. Therefore, this study focuses on the design and experimental investigation of a compact *Pueraria thomsonii* planter suitable for complex field conditions, aiming to improve planting efficiency, reduce labor intensity, and promote the mechanization of root crop planting.

## 2. Overall Design

In response to the engineering challenges of *Pueraria thomsonii* planting, including fragmented plots, limited operating space, and high dependence on manual labor, a functional decomposition

approach was adopted to divide the planting operation into basic functional units, namely soil drilling, seedling conveying and dropping, soil compaction, and irrigation. Based on this analysis, a compact integrated planter was designed, consisting of a soid-drilling device, a *Pueraria thomsonii* Benth root storage device, a soil-compacting device, a seedling conveying and dropping device, and an irrigation device. These functional mechanisms were arranged in a modular layout to enable continuous completion of drilling, seedling placement, and soil compaction during a single forward movement.

Subsequently, three-dimensional modeling was performed to determine the overall structure and key design parameters. Mechanical calculations and simulation analyses were conducted on the critical mechanisms to verify the structural rationality and operational reliability of the proposed design, providing an engineering basis for subsequent prototype fabrication and experimental validation.

## 2.1 Main Structural Components of the Entire Machine

This mechanical design addresses the practical challenges of *Pueraria thomsonii* Benth cultivation by creating a compact *Pueraria thomsonii* Benth planter specifically tailored for complex field environments. The equipment integrates five core functional units: a soid-drilling device, a *Pueraria thomsonii* Benth root storage device, a soil-compacting device, a seedling conveying and dropping device, and an irrigation device. These devices are strategically arranged according to their distinct functions and operational sequence to form a complete *Pueraria thomsonii* Benth planter, as illustrated in Figure 1.

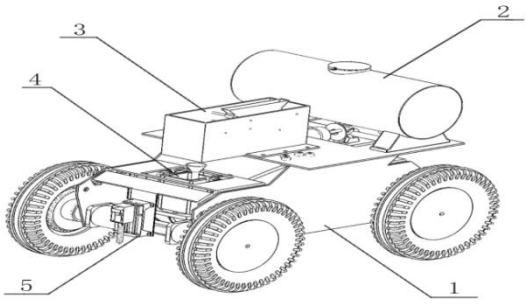


1. Vehicle body; 2.irrigation device; 3.Pueraria thomsonii Benth storage device; 4. Seedling delivery and planting device; 5.Drilling device

Figure 1: Schematic diagram of the overall structure of the powder Pueraria thomsonii Benth planter

The machine features a compact design and integrates five core units to adapt to complex field environments. The key technical parameters are listed in Table 1.

Table 1: Key Technical Parameters

| Item/Unit | Value |
|---|---|
| Overall Dimensions/mm | 1200×800×450 |
| Total Weight/kg | 45 |
| Plant Spacing/cm | 50 |
| Drilling Depth/mm | 75 |
| Seedling Height/cm | 9 |
| Seedling Diameter/cm | 0.5 |
| Power System/V | 12 |

## 2.2 Workflow Design

First, the front-mounted soil-drilling mechanism breaks through the soil with a high-speed rotating drill bit, forming regular planting holes. Immediately afterward, the soil-compacting device activates to ensure the soil conditions are suitable for the *Pueraria thomsonii* Benth seedlings to be placed. The seedling conveying and dropping device automatically calibrates the seedling's orientation, ensuring the bud point faces upward and drops vertically into the planting hole, eliminating the angle deviation issues associated with manual placement. The rear irrigation module connects to a detachable water tank, controlling drip irrigation volume via pressure sensors. It achieves ±50ml precision per plant, saving over 60% water compared to traditional flood irrigation. These four interconnected functions enable full-process *Pueraria thomsonii* Benth mechanization, with hourly efficiency reaching 800-1000 plants, which is more three times higher than that of manual operation.

## 2.3 Primary Functions and Structural Design of Key Components

### 2.3.1 Drilling Mechanism Design

The core function of the soil-drilling device is to drill precise holes in the soil-filled bags placed on the ridges. It consists of a three-axis linear slide table, an electric motor, and auger working in concert. Upon activation, the motor rapidly drives the auger to high-speed rotation. Simultaneously, the three-axis linear slide table precisely executes vertical movements according to a pre-programmed sequence. This mechanism enables precise control over the drill's feed depth [3], ensuring the hole depth perfectly match the planting requirements for *Pueraria thomsonii* Benth seedlings and laying a solid foundation for the subsequent healthy development of the *Pueraria thomsonii* Benth. The main configuration of the soil-drilling mechanism is illustrated in Figure 2.

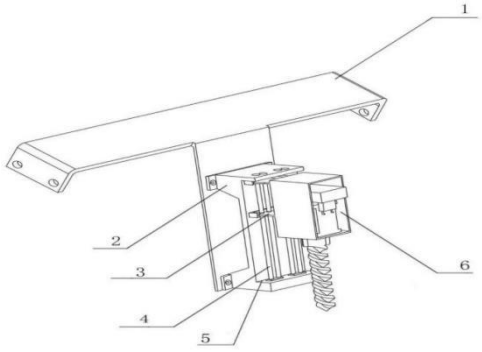


1.T-shaped support plate; 2.Lifting assembly; 3.Connecting support plate; 4.Connecting column; 5.Vertical groove; 6.Rotary drilling rig

Figure 2: Schematic diagram of soil-drilling mechanism

In the design of hole-digging drill bit, the helix angle α formed between the spiral blades and the horizontal plane is one of the core parameters. The magnitude of the helix angle α significantly impacts the bit's power consumption and operational intensity. Therefore, determining a reasonable value of the helix angle α has become a crucial technical approach for balancing the bit's energy efficiency and operational performance [4-5]. Based on the relationship between lead and helix angle: $h = \pi D \tan \alpha$, the helix angle of the blade is calculated as $\alpha = 12.86$ °. Within the specified range, this value meets the requirements.

Within this mechanism, the drill bit feed depth is controlled through the coordinated operation of the electric motor driving the auger and the slide table executing vertical movements. The key

parameters of drill bits are listed in Table 2.

Table 2: Key Parameters of Drill Bits

| Name | Diameter | Rise Angle | Rotational Speed | Length | Feed Rate |
|---|---|---|---|---|---|
| Value | 12 mm | 12.86 ˚ | 3.84 rad/s | 300 mm | 10 mm/s |

### 2.3.2 Force Calculation and Analysis of the Drill Mechanism

During operation, the key force-bearing processes include: the drill bit entering the soil, and the rotating blade entering and exiting the soil.

Formula for the force obstructing the drill bit's penetration into soil:

$$F_{Z1}=(q+kS)D_1 \quad (1)$$

Where: q is the soil-related coefficient, with the unit of kN/m; k is the inherent soil-related coefficient, with the unit of $kN/m^2$; S is the feed value per revolution of the drill bit, with the unit of mm/r; $D_1$ is the numerical value of the drill bit's diameter, with the unit of mm. Calculations yield: $F_{z1}$=470.4 *N*.

For the rotating blade entering the soil, $q_0$=2.0 *kN/m*, $k_0$=200 $kN/m^2$ are selected. The caculation formula is as follows:

$$F_{z2}=2[q_0 \sin\varphi - k_0 S\cos(\delta+\theta)]\int_{\frac{D_1}{2}}^{\frac{D}{2}} dr \quad (2)$$

Where: $q_0$ represents the soil proportional resistance coefficient, with the unit of kN/m; φ denotes the angle between the soil penetration resistance and the horizontal plane, with the unit of β/°; $k_0$ represents the soil deformation resistance coefficient due to squeezing effects, with the unit of $kN/m^2$; θ is the friction angle between the soil and the blade, with the unit of β/°. Substituting parameters yields: $F_{z2}$= 162.56 N.

For the rotating blade entering the soil, the calculation formula is as follows:

$$F_{z3}=H\pi(\tfrac{D}{2})^2\rho_1/\cos\alpha \quad (3)$$

Where: $\rho_1$ represents the soil density value. According to relevant literature [6], the density of this soil type is typically $1.4\times10^3$ $kg/m^3$; α refers to the value of the helical rise angle, and $F_{z3}$ is taken as 14.86. Through the above analysis and calculation,$F_{z3}$≈11.29 *N*. During the drill's hole-digging operation, the variation range of $F_{z3}$ is 0～11.29 N. Considering practical operational requirements and safety considerations, the maximum value of 11.29 N is directly adopted as the basis for calculation.

Therefore, the total resistance during the drill's penetration into the soil is as follows:

$$F_z=F_{z1}+F_{z2}+F_{z3}=644.25\ N \quad (4)$$

In summary, the total torque calculation of the drill bit during operation is as follows:

$$M_0 = M_1 + M_2 + M_3 \quad (5)$$

$$M_1=F_{z1}+D_1 \quad (6)$$

$$M_2=F_{z2}(\frac{D-D_1}{2}) \quad (7)$$

$$M_3=F_{z3}Sn \quad (8)$$

Where: $M_1$ is Drill bit torque; $M_2$ is Blade torque; $M_3$ is Torque during soil lifting by spiral

blades; n-Number of blade revolutions, taken as 4.5; Substituting the values into calculation, the total torque $M_0$=94.8122 N·m is obtained.

Ultimately, the power required for driving the drill bit is calculated by the following formula:

$$N=M_0nk/716.2 \quad (9)$$

Substituting yields N=1.98 kW. Based on relevant data[7], this study verified through field tests that this parameter can meet the drilling requirements in complex soil conditions, further confirming the rationality of selecting a drill bit with a power rating of 2 kW or higher in this design.

### 2.3.3 Design of the Soil-Compacting Mechanism

The soil-compacting mechanism primarily secures the saplings. Through a double rack-and-pinion mechanism, the soil-compacting mechanism performs reciprocating vertical motion. By controlling the soil-compacting tubers to move horizontally along its guide rails, the mechanism straightens the *Pueraria thomsonii* Benth tubers that have fallen into the bags and applies sufficient force to fix the *Pueraria thomsonii* Benth tubers firmly in the soil. In this way, when the *Pueraria thomsonii* Benth seedlings are placed, they can obtain stable support, effectively preventing the seedlings from falling over and providing a strong guarantee for the smooth growth of the *Pueraria thomsonii* Benth seedlings. The schematic diagram of the soil-compacting mechanism is shown in Figure 3.

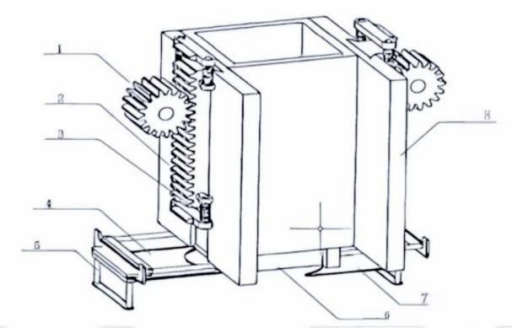

1.Gear assembly; 2. Rack-and-pinion transmission mechanism; 3. Spring; 4. Soil-gathering plates; 5. Height adjustment mechanism; 6. Soil-compacting plate; 7. Soil-gathering plate; 8.Housing

Figure 3: Schematic diagram of the top soil mechanism

Within this mechanism, the movement of the thrust mechanism is coordinated through a rack-and-pinion assembly to control its vertical motion. The combined parameters are listed in Table 3.

Table 3: Combined Parameters for Gear and Rack

| Property | Value | Unit |
|---|---|---|
| Gear module m | 4 | - |
| Number of teeth Z | 20 | - |
| Gear width b | 30 | mm |
| Gear material | 45 steel | - |
| Allowable contact stress[$\sigma_H$] | 550 | MPa |
| Allowable bending stress[$\sigma_F$] | 250 | MPa |
| Gear pitch diameter$d_1$ | 80 | mm |

### 2.3.4 Stress Calculation and Analysis of the Soil-Lifting Mechanism

In this mechanism, the Hertz contact theory needs to be used to verify the contact strength, and

the formula is as follows:

$$\sigma_H = Z_E \sqrt{\frac{F_t \cdot K_A \cdot K_V \cdot K_{H\beta}}{b \cdot d_1}} \tag{10}$$

Where: $Z_E$ is the material elastic coefficient. Since 45 steel is used as the material, $Z_E$=189.8. $F_t$ is the tangential force; $K_A$ is the load coefficient, $K_A$= 1.3; $K_V$ is the velocity coefficient, $K_V$= 1.1; $K_{H\beta}$ is the impact and tooth-direction load distribution coefficient, $K_{H\beta}$= 1.2. Substituting the values into Formula (10), $\sigma_H$=569.4 *MPa* is verified, which satisfies $\sigma_H < [\sigma_H] = 550$ *MPa*.

For the components of this mechanism, the bending strength of the soil-reinforced panels must be verified. Key parameters of the soil-gathering panels are listed in Table 4.

Table 4: Key Parameters of Soil-Gathering Plate

| Property | Value | Unit |
|---|---|---|
| Length of the Soil-Gathering Plate L | 500 | mm |
| Cross-section Width b | 100 | mm |
| Height h | 20 | mm |
| Material | Q235 | - |
| Allowable Bending Stress $\sigma_b$ | 160 | MPa |
| Soil Backfilling Resistance | 2000 | N |

Substitute the data from Table 4 into the bending stress calculation formula:

$$\sigma_b = \frac{F \cdot L}{(b \cdot h^2)/6} \tag{11}$$

The result is $\sigma_b$=0.15 MPa, meeting the design requirements.

Additionally, an analysis of the compaction plate's load is required. Considering the growth conditions of *Pueraria thomsonii* Benth, the soil during planting is typically dry soil, yielding a soil unit area resistance p can be taken between 30–60 kPa; and 40 kPa is used in this calculations. The soil-compacting plate has an irregular shape, with its area measured at 0.15$m^2$. Therefore, the compaction resistance $F_s$ is caculated as follows:

$$F_s = p \cdot A \tag{12}$$

Obtained: $F_s$=6000 N.

In this system, the mass m = 10 kg, g=9.8 m/s$^2$, acceleration a=0.5 m/s$^2$, and the coefficient of friction is μ=0.2. Through the following formulas:

$$F_g = m \cdot g \tag{13}$$

$$F_i = m \cdot a \tag{14}$$

$$F_f = \mu \cdot m \cdot g \tag{15}$$

The self-weight of the soil-compacting plate $F_g$= 98N, inertial force $F_i$=5N, and friction force *Ff* = 19.6 N are calculated through Formulas (13), (14), and (15) respectively. Therefore, the total vertical load of the soil-compacting mechanism is:

$$F = F_s + F_g + F_i + F_f = 622.1 \tag{16}$$

The total vertical load of this design is 622.1 N, and the gear contact stress is 569.4 MPa. According to relevant research[5], this is close to the result that the gear contact stress is 565 MPa under a 620 N load, and both are less than the allowable stress, verifying the rationality of the structural strength.

## 3. Key Mechanism Simulation Verification

Three-dimensional modeling of the drill bit was performed using SolidWorks, with finite element analysis applied solely to the drill bit. During the modeling process, certain secondary factors that have little impact on the results were ignored [8], excluding residual stresses caused by manufacturing defects and neglecting deformation and other flaws arising from CNC machining of metal components. The suitability of material selection and structural design for operational requirements was validated by applying forces to the drill bit.

### 3.1 Finite Element Analysis of Stiffness and Strength

First, configure the material settings. The drill bit material is structural steel, with its performance parameters listed in Table 5.

Table 5: Structural Steel Performance Parameters

| Attribute | Value | Unit |
|---|---|---|
| Material Density | 7.85E+3 | $kg \cdot m^{-3}$ |
| Young's Modulus | 2E+11 | Pa |
| Bulk Modulus | 1.667E+11 | Pa |
| Shear Modulus | 7.6923E+10 | Pa |
| Poisson's Ratio | 0.3 | - |

The mesh convergence was determined by plotting the maximum stress under a 100 N load during steady-state mechanical analysis against the number of mesh elements, with the final mesh selected based on computational accuracy. Boundary conditions specified zero displacement in the Z-direction at the bottom and fixed the center point. Table 5 lists the six selected mesh sizes [9]. The mesh configuration for the drill bit is shown in Figure 4.

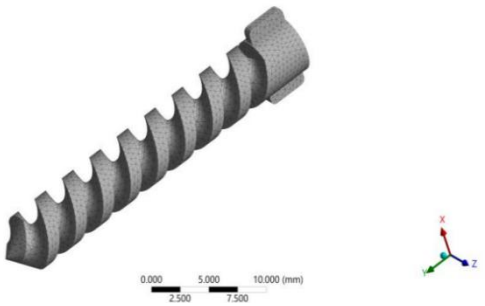


Figure 4: Drill bit grid division diagram

During the simulation process, as the number of grid cells continuously increases, the maximum stress gradually rises and eventually stabilizes within a range of approximately 290 MPa. Throughout this process, the stress distribution trend on the drill bit remains consistent, concentrating at the central tip of the bit. Based on the actual operating conditions of the drill bit, constraints and loads were applied to its finite element model. According to literature review [10], a load of 300 N was applied to the left end face of the drill bit.

Under a load of 300 N, the structural displacement of the drill bit occurs only at the bit tip, with a displacement distance of 0.0116 mm—far smaller than the drill bit's own dimensions, as shown in Figure 5. Furthermore, as shown in Figure 6, the stress-strain analysis indicates that stresses and strains are primarily concentrated at the tip of drill bit, with a maximum stress of 132.59 MPa—significantly below the material's yield strength of 335 MPa. Consequently, the drill design for this device meets the equipment's strength and stiffness requirements of the equipment.

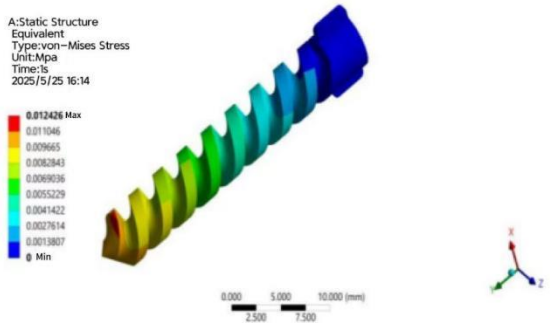


Figure 5: Drill bit displacement

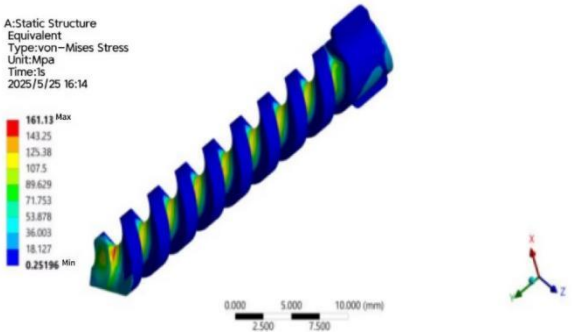


Figure 6: Drill stress and strain

### 3.2 Life and Fatigue Finite Element Analysis

After verifying the stiffness and strength of the drill bit, fatigue analysis and life prediction must also be conducted. By testing the relationship between stress amplitude and fatigue life (number of cycles) of the material under symmetrical cyclic loading, it was found that the stress-strain curve exhibits a logarithmic linear decline trend. This indicates that fatigue life can be significantly extended when stress amplitude is reduced.

The loaded curve based on zero-load and mean stress theory plots mean stress *Sm* on the horizontal axis and the ordinate representing the allowable alternating stress amplitude *Sa*. The curve boundaries represent the fatigue limit combinations for materials under different mean stresses. In actual working conditions, the mean stress, residual stress, or static load must be corrected before calculation to ensure reliable fatigue life prediction. Here, *Sa* denotes the alternating stress amplitude (cyclic stress amplitude), *Se* represents the material's fatigue limit, *Sm* is the mean stress, and *Su* is the material's tensile strength. Under the condition of a force F = 300 N applied to structural steel, the tensile strength *Su* = 600 MPa, and the fatigue limit is taken as *Se* = 0.45 × *Su* = 270 MPa.

By substituting the above data for verification, it was found that the current working condition points (3.82, 268.8) are located in the safe area below the curve, indicating that the design of this mechanism is reasonable.

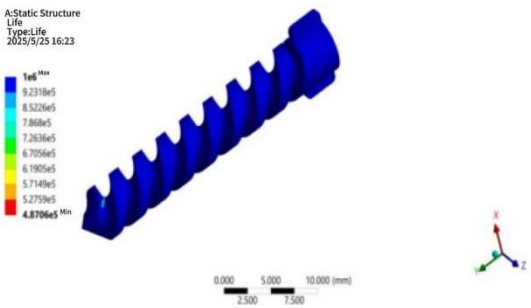


Figure 7: Lifetime cloud diagram

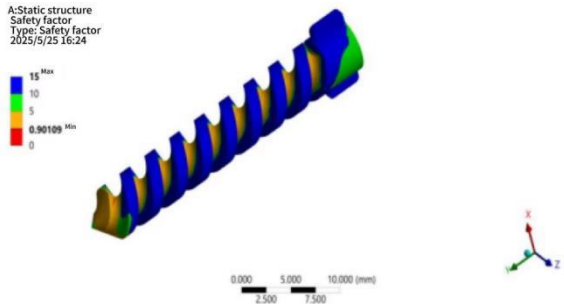


Figure 8: Security factor cloud diagram

In the fatigue life map (Figure 7), through the comparison of color gradients, it can be observed that red areas (such as the drill bit head) indicate the lowest fatigue life. This is caused by high stress concentrations resulting from geometric discontinuities. The transition from red to blue signifies progressively increasing fatigue life, with blue areas indicating the material can withstand a higher number of cycles under the same load. This directly highlights structural weak points of the structure. Upon verification, the design of this mechanism is reasonable.

The generated safety factor cloud diagram is shown in Figure 8, representing the fatigue safety

margin of each structural region using dimensionless values. Values <1 (red regions) indicate that actual stresses exceed the material's fatigue strength, posing a failure risk; values >1 (blue regions) indicate design safety. The drill head exhibits the lowest safety factor, aligning with high-risk areas in both the life expectancy and damage distribution maps, thereby validating the multidimensional consistency of the analysis results.

## 4. Prototype Testing

Using the preliminary design of the Pueraria thomsonii Benth planter as a reference, a three-dimensional model was created in SolidWorks software. This model was then compared with the results of finite element analysis to verify the feasibility of the design and the accuracy of the analysis outcomes.

### 4.1 Prototype Development

The assembled prototype primarily consists of a planting system and a chassis section. The planting system is further divided into a soil-drilling device, a seedling-placement device, and a soil-lifting device. All three devices are supported by aluminum extrusions and secured to the chassis. The aluminum chassis offers high load-bearing capacity and robust structural integrity. The control module and power supply are installed in the open space above the chassis. The completed experimental prototype serves to verify various functions, with its key parameters listed in Table 6.

Table 6: Prototype Key Parameters

| Items | Parameters |
|---|---|
| Dimensions | 1000 mm×500 mm×400 mm |
| Support Frame | Aluminum and Wooden Boards |
| Controller | STC89C52 |
| Power Supply | 12V |

### 4.2 Prototype Functional Testing

To validate the core functions of the compact *Pueraria thomsonii* Benth planter, an approximate grassland was selected as the test site in the absence of actual *Pueraria thomsonii* Benth cultivation planting field. The site is a regular rectangle measuring 2 m by 10 m. The test prototype operated at a forward speed of 0.1 m/s, with planting spacing set at 50 cm and drilling depth at 10 cm. To simulate *Pueraria thomsonii* Benth seedlings, wooden sticks measuring 5-6 cm in length and 4 mm in diameter were used as substitute planting material. The test focused on evaluating the drilling, soil-compacting, and seedling-placement capabilities.

This simulation test comprised five test sets, with each set representing one planting process. The recorded durations are shown in the table 7.

Table 7: Planting Schedule Record

| Test No. | Drilling (Up/Down)/s | Soil Compacting (Up/Down)/s | Seedling Placement/s | Total Duration/s |
|---|---|---|---|---|
| 1 | 30 | 20 | 5 | 55 |
| 2 | 31 | 21 | 6 | 58 |
| 3 | 31 | 19 | 5 | 55 |
| 4 | 29 | 20 | 5 | 54 |
| 5 | 29 | 21 | 6 | 56 |

From the above data, it can be seen that the planting time of each group is within one minute. Taking the test site as an example, according to the set spacing, if planting is carried out in the entire set area, the expected maximum number of plantings is 20, and the total planting time is 1200 s. Thus, the maximum planting efficiency is 1.1 m⁻¹min, which meets the expected efficiency requirements.

## 5. Conclusion

To enhance *Pueraria thomsonii* Benth planting efficiency and reduce labor intensity, this paper addresses the issue of low mechanization in *Pueraria thomsonii* Benth cultivation by designing an integrated *Pueraria thomsonii* Benth planter featuring hole-drilling, bag-opening, seedling-placement, and irrigation functions. Detailed designs were implemented for key components such as the hole-digging device and seedling-storage mechanism. Through rigorous stress analysis and precise mathematical calculations, optimal components including drill bits, motors, and conveyor belts were selected to maximize the planter's operational efficiency. This design offers valuable insights for developing automated and intelligent *Pueraria thomsonii* Benth planter.

## Acknowledgments

This work was supported by the National College Student Innovation Training Program (Project No.: 202410595031).

## References

*[1] Wu Xiaoyu. Preliminary Study on Simplified and Efficient Cultivation Techniques for Pueraria lobata in Guangxi [J]. Southern Horticulture, 2024, 35(03): 61-64.*
*[2] Du Xinxiao, Cao Sheng, Long Ziyuan, et al. Analysis of Current Cultivation Status and Economic Benefits of Pueraria lobata in Tengxian County, Guangxi [J]. China Vegetable, 2022, (11): 110-114.*
*[3] Xu Zheng, Hu Xing, Chen Hui, et al. High-Yield Cultivation Technology for Pueraria lobata with Plastic Mulch in Tengxian and Pinghe, Yangtze River Basin—Part II of the Series on Cultivation of New and Superior Vegetables in the Yangtze River Basin [J]. Science of Planting and Breeding, 2014, (12): 26-28.*
*[4] Jiang Quanshan. Design of Tree-Planting Hole Digger [J]. Forestry Machinery and Woodworking Equipment, 2006, (05): 24-25+28.*
*[5] Jiao Ruibin, Wang Rui, Shi Huifeng, et al. Design of 1WK-70 Twin-Screw Blade Tree-Planting Hole Digger [J]. Xinjiang Agricultural Mechanization, 2020, (03): 31-33.*
*[6] Xu Yuezhen, Wang Yan, Zheng Debo, et al. Cadmium Accumulation Characteristics and Yield Differences of Local Pueraria Lobata Varieties Under Cadmium Stress [J]. Seeds, 2024, 43(09): 48-52+85.*
*[7] Wang Xiyi, Qin Weilun, Yuan Rendda, et al. Design of a Small Potato Planter Seeding System [J]. Modern Agriculture, 2022, (08): 94-96.*
*[8] Sun, Y. J., Yang, F. Z., & Wang, J. (2019). Mechanical modeling and verification of the rack-and-pinion soil-compacting mechanism for root crop planters. Journal of Mechanical Design, (7), 10-15.*
*[9] Hou Rongguo, Wang Xiangtian, Lu Ping, et al. Design of Full-Process Integrated Tree-Planting Engineering Vehicle and Its Key Components [J]. Mechanical Design and Manufacturing, 2021, (10): 62-65.*
*[10] Kang Yu. Research on Moisture Diffusion Reliability and Injection Molding Process of Plastic-Sealed Devices [D]. Xi'an University of Electronic Science and Technology, 2020.*